Article

Bioorthogonal DNA Adsorption on Polydopamine Nanoparticles Mediated by Metal Coordination for Highly Robust Sensing in Serum and Living Cells

Yingcai Meng, Peng Liu, Wenhu Zhou, Jinsong Ding, and Juewen Liu

ACS Nano, **Just Accepted Manuscript** • DOI: 10.1021/acsnano.8b03019 • Publication Date (Web): 21 Aug 2018

Bioorthogonal DNA Adsorption on Polydopamine Nanoparticles Mediated by Metal Coordination for Highly Robust Sensing in Serum and Living Cells

Yingcai Meng,[†] Peng Liu,[†] Wenhu Zhou,[*,†] Jinsong Ding,[*,†] Juewen Liu[‡]

[†]Xiangya School of Pharmaceutical Sciences, Central South University, Changsha, Hunan, China, 410013.

[‡]Department of Chemistry, Waterloo Institute for Nanotechnology, University of Waterloo, Waterloo, Ontario, Canada, N2L 3G1.

*Email: zhouwenhuyaoji@163.com

Abstract

DNA-functionalized nanomaterials, such as various 2D materials, metal oxides, and gold nanoparticles, have been extensively explored as biosensors. However, their practical applications for selective sensing and imaging in biological samples remain challenging due to interference from sample matrix. Bioorthogonal chemistry has allowed specific reactions in cells, and we want to employ this concept to design nanomaterials that can selectively adsorb DNA but not proteins or other abundant biomolecules. In this work, DNA oligonucleotides were found to be adsorbed on polydopamine nanoparticles (PDANs) *via* polyvalent metal-mediated coordination, and such adsorption bioorthogonally resisted DNA displacement by various biological ligands, showing better performance compared to graphene oxide and metal oxide nanoparticles for DNA detection. Using DNA/PDANs as biosensors, a detection limit of <1 nM target DNA was achieved in serum and other biological samples, and imaging of cancer-related microRNA in cells was demonstrated. The DNA binding mechanism on PDAN was further studied by ligand displacement experiments and X-ray photoelectron spectroscopy (XPS) characterization, which demonstrated the critical role of polyvalent metal ions to bridge DNA with PDANs. This work provides fundamental insights into the biointerface science of PDANs with DNA, which can benefit applications in biosensor design, directed assembly of nanomaterials, bioimaging, and drug delivery.

Keywords: polydopamine, DNA, metal coordination, biosensors, cancer

Bioorthogonal chemistry allows specific reactions in cells for labeling designated biomolecules, and this strategy has profoundly impacted bioimaging and diagnosis.[1, 2] However, developing bioorthogonal surfaces that can selectively adsorb only one type of biomolecule remains challenging. For example, DNA-functionalized surfaces have been extensive studied, eliciting a diverse range of applications in nanomaterial assembly,[3-6] biosensor development,[7-11] and drug/gene delivery.[12, 13] Various nanomaterials, such as metallic nanoparticles,[14] metal oxide nanoparticles,[15-17] semiconductor quantum dots,[18] and nanoscale carbon materials,[19, 20] have been explored. Interestingly, most of these nanomaterials possess a strong fluorescence quenching ability, which allows their application for fluorescence-based DNA sensing.[7-11]

While such simple and elegant sensors are highly sensitive and selective in clean buffers, sensing in biological fluids is difficult due to non-specific DNA displacement by proteins or other biomolecules, causing false positive signals.[21] DNA has two main components responsible for its adsorption: the nucleobases and the phosphate backbone. For example, DNA uses its nucleobases to adsorb on graphene oxide (GO) through π-π stacking and hydrogen bond,[22, 23] while its adsorption on metal oxide nanoparticles relies on the phosphate backbone (*e.g.* electrostatic interactions and Lewis acid/base interactions).[15, 16] However, these binding forces are all susceptible to competition from biomolecules.[15, 24-26] To solve this problem, Tan and coworkers introduced a non-sensing probe with a different fluorophore label as an internal standard to account for non-specific probe displacement.[27] In addition, covalent probe conjugation was also attempted,[28] but the simplicity of physisorption was lost. Therefore, it remains a challenge to find a surface for bioorthogonal adsorption of DNA.

Metal coordination is an important mechanism for building materials,[29] while its application in DNA adsorption was rarely explored. Recently, polydopamine (PDA), a synthetic analogue of natural melanin produced by autoxidation of dopamine (DA), has attracted a lot of attention. Because of its ease of synthesis, excellent biocompatibility and biodegradability, and surface coating properties, PDA has been

widely used for drug delivery, photothermal therapy, tissue engineering, cell adhesion and biosensing/bioimaging.[30-33] PDA nanoparticles (PDANs) can adsorb DNA and quench fluorescence,[34] allowing related analytical applications.[34-38] PDA is also an excellent metal ligand,[39-42] and we reason that it might be a useful platform for developing coordination based DNA adsorbing materials.

Herein, we studied DNA adsorption by PDANs, and found the importance of metal coordination mediated DNA adsorption. Among various tested nanomaterials, only PDANs resisted DNA displacement by biological ligands. Therefore, DNA was orthogonally adsorbed on PDANs enabling highly robust DNA sensing in various biological samples including serum and living cells. A detailed study on the adsorption mechanism was also performed.

Results and Discussion.

Ca^{2+}-mediated DNA adsorption. Our PDANs were synthesized by using a literature reported method (Figure 1A),[43] and were characterized by UV-vis, Raman and IR spectroscopy (Figure S1A, B, C), all supporting successful preparation of PDANs.[44] The diameter of the PDANs was ca. 160 nm as measured by DLS (Figure S1D). From TEM, the PDANs were spheres and the particle size was consistent with the DLS measurement (Figure 1B). For comparison, we also included a metal oxide (ZnO, Figure 1C) and a carbon-based material (GO, Figure 1D) in this study. DNA uses its nucleobases to bind to GO,[22, 23] while its phosphate backbone to interact with ZnO.[15, 16] We hope that PDAN can use a different mechanism to achieve more stable adsorption in a biological sample matrix.

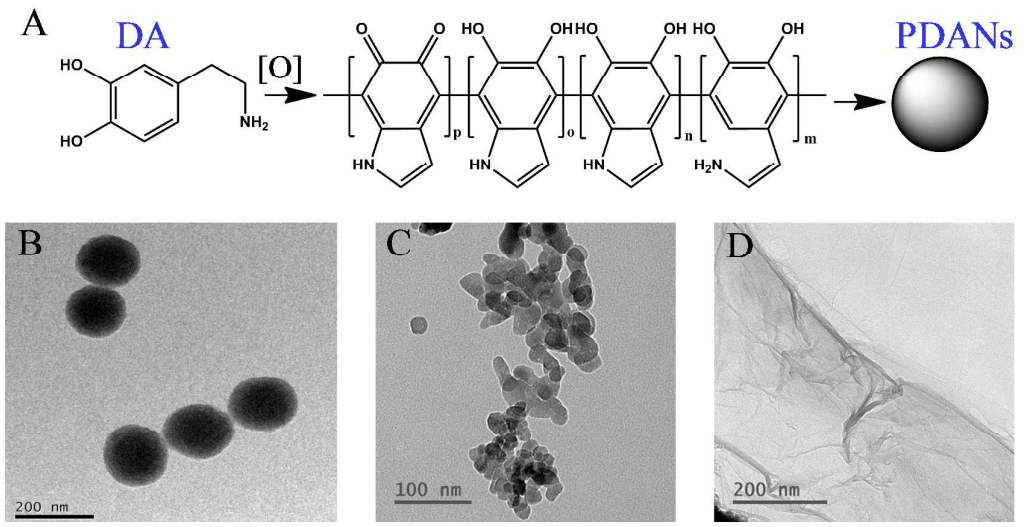

Figure 1. (A) A scheme showing the synthesis process of PDANs by oxidation of DA. TEM micrographs of (B) PDANs, (C) ZnO, and (D) GO used in this work.

We first optimized the condition for DNA adsorption. PDANs can efficiently quench different kinds of fluorophores.[34] Therefore, with fluorescently labeled DNA, the kinetics of DNA adsorption was conveniently monitored based on the extent of fluorescence decrease. A 6-carboxyfluorescein (FAM)-labeled 15-mer DNA homopolymer comprised of just A base (*i.e.* A_{15}) was employed.

Since DNA is a polyanion due to its phosphate backbone, the surface charge of PDANs would be likely to influence their interactions. The PDANs were negatively charged over the pH range of 3-8 attributed to the surface catechol groups (Figure S2). Therefore, the PDANs were not expected to spontaneously adsorb DNA due to charge repulsion. Salt is known to screen charge repulsion, and can promote DNA adsorption on negatively charged gold nanoparticles,[45, 46] and GO.[15, 21] Here, we also studied DNA adsorption as a function of salt concentration. However, we failed to observe DNA adsorption or fluorescence quenching by adding up to 200 mM Na^+ (Figure 2A) or K^+ (Figure 2B), although such a high salt concentration was sufficient to drive DNA adsorption on gold nanoparticles and GO. This suggested that the attractive force between DNA and PDANs was probably not strong enough.

Since the catechol groups of dopamine interact strongly with divalent metal ions,

we carried out the adsorption experiment using Mg^{2+} and Ca^{2+}. A slight fluorescence drop was observed with 1 mM Mg^{2+} (Figure 2C), suggesting adsorption of a small fraction of DNA (~10%). With 2 mM Mg^{2+}, 30% DNA was adsorbed after 30 min of incubation. Interestingly, Ca^{2+} was even more effective than Mg^{2+} for DNA adsorption, and an obvious fluorescence decrease was observed with just 0.5 mM Ca^{2+} (Figure 2D). With 2 mM Ca^{2+}, the adsorption rate was very fast, and over 85% DNA was adsorbed within 1 min. Control experiments confirmed that Mg^{2+} and Ca^{2+} did not quench the fluorophore on their own (Figure S3).

Since Ca^{2+} and Mg^{2+} are biologically relevant metals, they might support DNA adsorption in biological fluids. We then measured the capacity of DNA adsorption in the presence of 2 mM Ca^{2+}. A higher initial DNA concentration gave rise to more DNA adsorption, and the Langmuir isotherm can be used to fit the data, suggesting monolayer DNA adsorption, and a DNA adsorption/desorption equilibrium on PDANs surface. With 2 μM DNA added, a saturated loading of ~300 nM DNA was achieved with 100 μg/mL of PDANs (Figure 2E). Since DNA adsorption was achieved in the presence of Ca^{2+}, we further studied Ca^{2+}-dependent DNA loading (Figure 2F). DNA adsorption was promoted with higher Ca^{2+} concentrations, and saturated DNA loading was obtained with 10 mM Ca^{2+} (Figure 2F). This result further confirmed the critical role of Ca^{2+} for DNA binding.

We further explored the mechanism of DNA binding by tuning the length and sequence of DNA. The effect of DNA sequence was studied by using 15-mer DNA homopolymers (Figure 2G), and the adsorption capacity followed the order of $C_{15} \approx G_{15} > T_{15} \approx A_{15}$. Therefore, the nucleobase had a strong effect on DNA adsorption, and the higher capacities of C_{15} and G_{15} could be explained by their stronger coordination with Ca^{2+}, or their tendency to form folded structures such as G-quadruplex and i-motif to occupy less footprint on the surface. We then varied the length by using poly-A DNAs, and the loading decreased with longer DNA (Figure 2H). Therefore, the DNAs were adsorbed lengthwise instead of adopting an upright conformation.

The catechol of PDANs is a strong metal ligand. One classic example is

Fe^{3+}-catechol coordination to form revisable and pH-responsive crosslinks, which has found applications for preparing films, self-healing polymers, and Fe^{3+} detection.[39, 40, 47, 48] With Ca^{2+} coordination, the nucleation of hydroxyapatite on PDANs was promoted.[32] Many other divalent metals (*e.g.*, Mn^{2+}, Cu^{2+}, Zn^{2+}) were also reported to coordinate with catechol groups.[41, 42, 49] In our study, DNA adsorption was significantly promoted by Ca^{2+}. We reason that the surface properties of PDANs might be altered by Ca^{2+} coordination (*i.e.* Ca^{2+} doped surface), which in turn facilitated DNA binding. While the DNA adsorption can also be achieved by lowering the system pH with a completely different mechanism (Figure S4),[50] this Ca^{2+}-mediated method is more physiological relevant for biological applications.

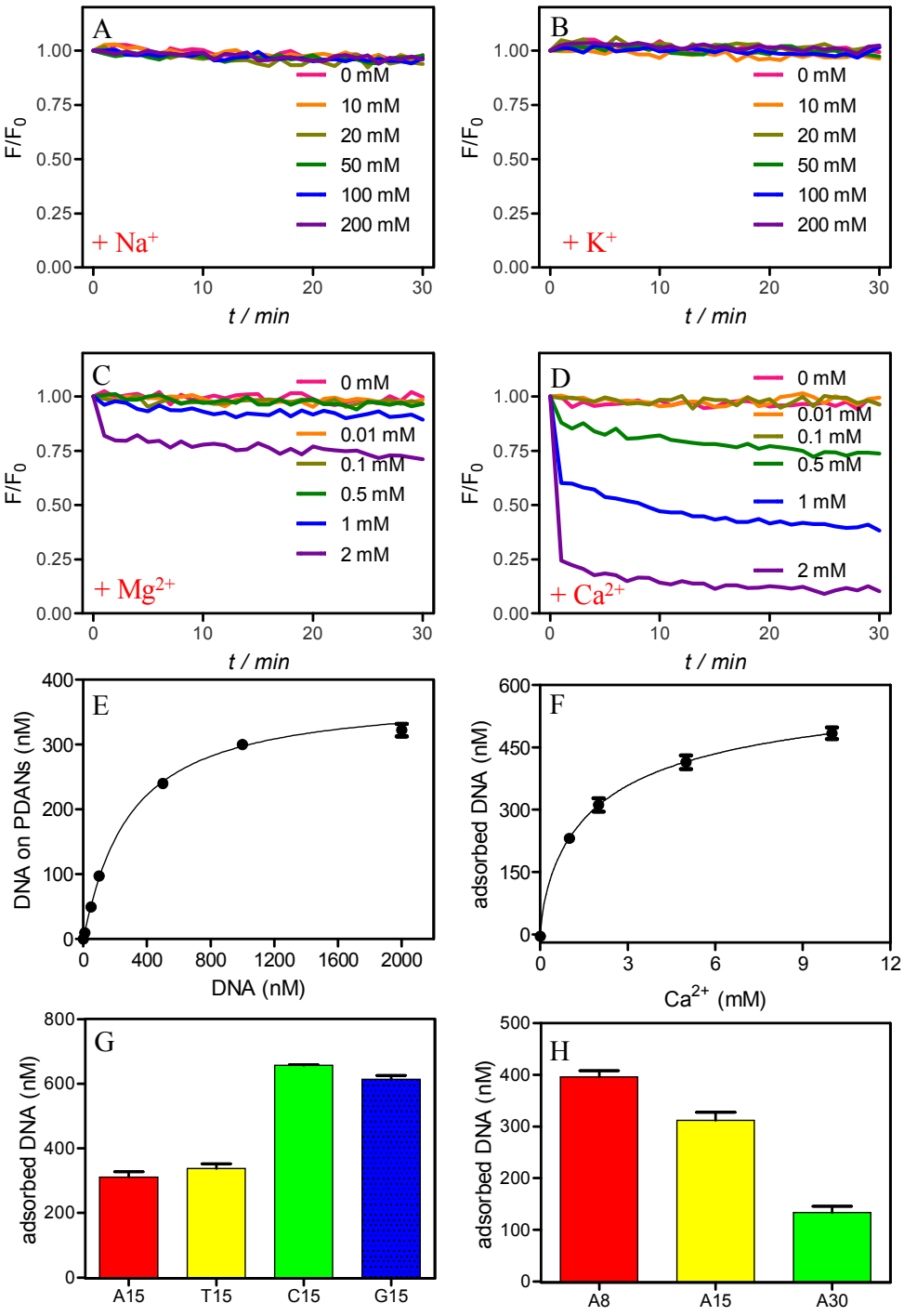

Figure 2. The adsorption kinetics of FAM-labeled A_{15} DNA by PDANs as function of (A) Na^+, (B) K^+, (C) Mg^{2+} and (D) Ca^{2+} concentration monitored by fluorescence decrease. DNA loading capacity (E) in the presence of 2 mM Ca^{2+} with various concentrations of DNA, and (F) as a function of Ca^{2+} concentration. The effect of (G)

DNA base and (H) DNA length on DNA loading capacity. The PDAN concentration was 50 μg/mL for (A-D), and 100 μg/mL for (E-H).

Highly robust DNA adsorption in biological matrixes. To date, various nanomaterials have been demonstrated for DNA detection based on the method in Figure 3A. A fluorescently labeled DNA probe is adsorbed with quenched fluorescence. This probe can be desorbed by adding its complementary DNA to form a duplex, while adding a non-targeting DNA is less effective, which is the basis for selective DNA detection. However, in biological samples, many other chemicals are presented and they may strongly compete with the probe DNA leading to false positive signals. Ideally, the probe DNA should be stably adsorbed and only dissociate by the target DNA. We then tested if PDANs can work for this purpose.

We first explored the stability of DNA adsorption in the presence of bovine serum albumin (BSA) as a model protein (Figure 3B). With 100 μg/mL BSA, almost no DNA desorbed from the PDANs after 1 h of incubation, suggesting a high stability. ZnO also resisted BSA displacement with only a moderate amount of DNA release, which is consistent with a previous report.[26] For GO, in contrast, more than 50% of the probe DNA detached. Therefore, BSA directly competed with the DNA on GO, which was likely due to the aromatic amino acid residues in BSA interacting with GO to dissociate the DNA bases.[51-53] A similar observation was also made when the systems were challenged with fetal bovine serum (FBS) (Figure S5). Therefore, PDANs and ZnO compared favorably to GO for resisting to protein-induced DNA dissociation.

In addition to proteins, both serum and cytoplasm contain a high level of phosphate species (~2 mM and ~30 mM, respectively).[54] Since DNA has a phosphate backbone, competition from phosphate was also tested (Figure 3C). A rapid and substantial DNA release was observed for DNA/ZnO upon addition of 10 mM phosphate. In contrast, the DNA was stably adsorbed on GO and PDANs in presence of phosphate.

Taken together, the stability of DNA adsorption by these three nanomaterials are

summarized in Figure 3D. GO was susceptible to protein displacement, and ZnO was susceptible to phosphate, while PDANs resisted both. Therefore, PDANs might be an optimal material for biological applications.

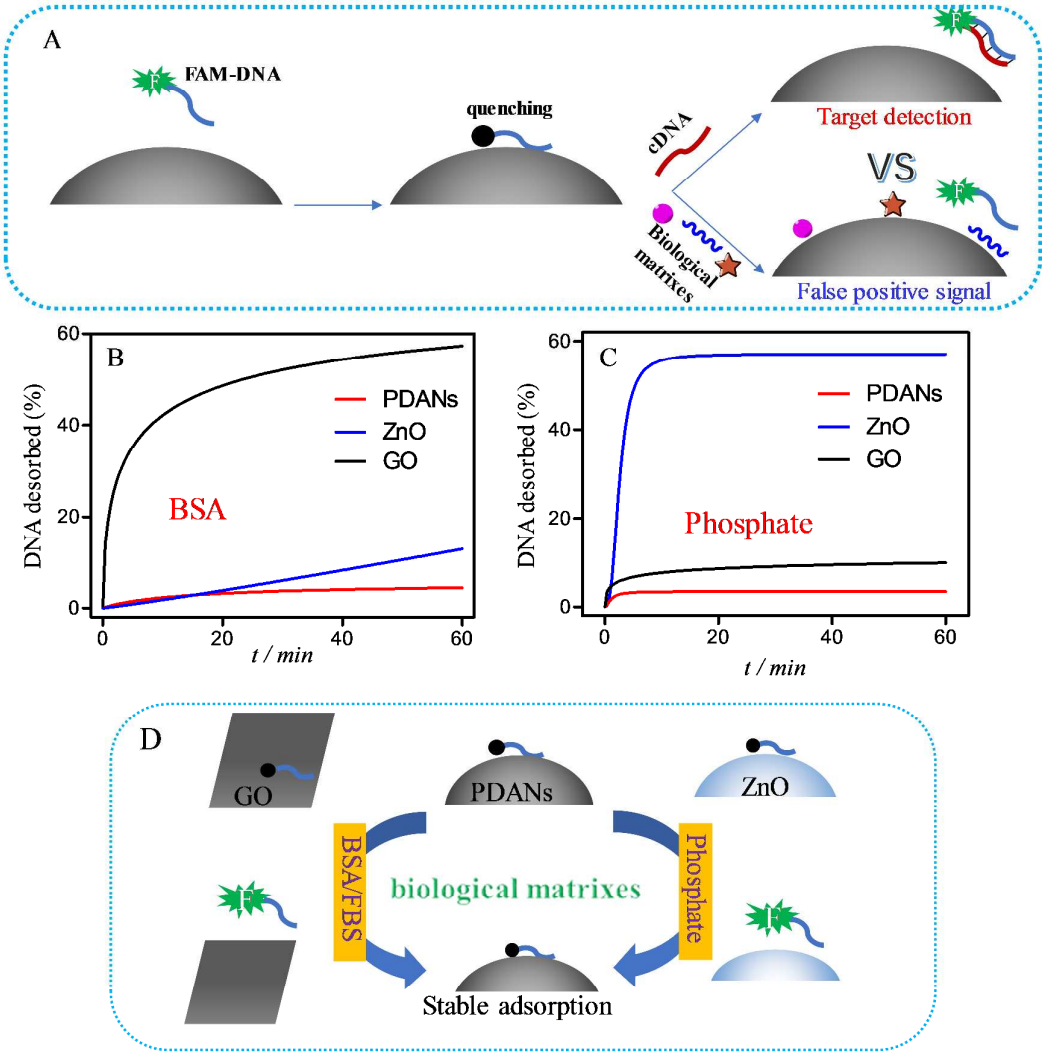

Figure 3. (A) The construction and application of DNA-based biosensors in biological samples. The quenched probe DNA can be desorbed by the intended target with a turn-on signal, while it may also be dissociated by other molecules in biological matrixes resulting in false positive signals. Fluorescence recovery of DNA/PDAN, DNA/ZnO and DNA/GO conjugates after adding (B) 100 μg/mL BSA, and (C) 10 mM phosphate. (D) A schematic diagram of PDAN, ZnO and GO probes in biological matrixes, and only the PDAN one can resist non-specific probe displacement.

Highly sensitive detection in buffers. Such highly stable DNA adsorption in biological matrixes prompted us to further study its analytical applications. Our sensing was based on the reaction in Figure 3A. A gradual fluorescence increase was observed after adding various concentrations of the complementary DNA as the target (Figure 4A), indicating the feasibility of quantitative detection. The detection limit (LOD) was calculated to be ~0.4 nM (3σ/slope), which is comparable to those of GO and ZnO.[26] We also studied specificity (Figure 4B), where the target DNA induced a much stronger signal than the single-base mismatched DNA (termed misDNA) did. None of the homo-DNAs (A_{15}, T_{15} and C_{15}) produced much signal, indicating high specificity.

We then applied the DNA/PDAN probe for DNA detection in various biological samples, including phosphate buffer, BSA, and serum (Figure 4C). In general, the sensor performance in these biological samples was quite comparable to that in the clean buffer, all showing a LOD of <1 nM. Therefore, the DNA/PDAN probe was robust enough for various biological applications.

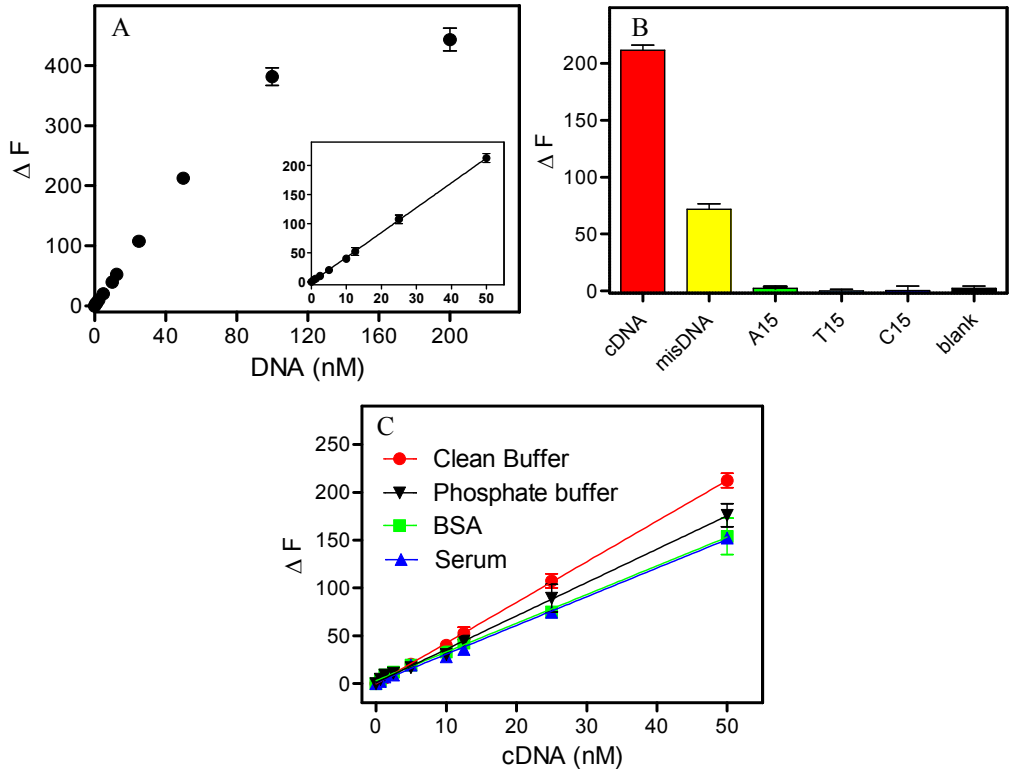

Figure 4. (A) The performance of the PDAN/DNA probe for cDNA detection (probe DNA = 50 nM). Inset: sensor linear response at low cDNA concentrations. (B) Specificity test of the PDAN/DNA probe with 50 nM different DNA sequences. (C) Detection of target DNA by the DNA/PDAN nanoprobe in clean buffer, 10 mM phosphate, 100 μg/mL BSA, and 0.5% serum.

Nanoprobes in living cells. Having demonstrated DNA detection in biological fluids, we then explored the DNA/PDAN in living cells for imaging tumor-related microRNA (miRNA). MiRNAs are a group of small non-coding RNAs with a typical length of 19-25 nucleotides important for regulating gene expression.[55] Recently, miRNAs have received much attention as cancer biomarkers. For example, miRNA-21 (miR-21) is an important oncogene overexpressed in many cancers,[56] and detection of miRNA-21 in living cells is important for tumor diagnostic.[57-59] As a proof-of-concept, the A549 lung cancer cell line was chosen, and the miRNA-21 level was first measured by real-time PCR. As shown in Figure S6, significant

overexpression of miRNA-21 in A549 cells was observed, which was over 10^5-fold higher than that in the RLE-6TN normal cells. The cytotoxicity of the nanoprobes was tested by the MTT assay (Figure S7). After 8 h of incubation, both A549 and RLE-6TN cells remained ~80% viability without obvious cell morphologic change (Figure S8), suggesting low cytotoxicity and good biocompatibility.

The cells were incubated with the nanoprobes for 8 h to allow internalization. Localization of cells was visualized by staining the cell nuclei in blue by DAPI (Figure 5), and the green fluorescence signified the release of probe DNA from nanoprobes. We first tested nanoprobes with A549 cancer cells (Figure 5A). From the confocal microscopy, strong green fluorescence was observed for all of the three nanoprobes (*i.e.* DNA/GO, DNA/ZnO and DNA/PDANs), suggesting substantial probe DNA dissociation. However, non-specific fluorescence increase could occur to produce false positive signal.

To explore whether the turn-on fluorescence was from the miR-21 target, we also used the RLE-6TN normal cells as a negative control (Figure 5B). The miR-21 level in the RLE-6TN cells was very low as measured by PCR. Interestingly, substantial green fluorescence was still observed for GO and ZnO, while the signal from the PDAN probe was at the background level. The fluorescence intensities of the probes in both types of cells were quantified in Figure 5C. Three probes displayed a comparably high intensity in the A549 cells, while only PDANs showed a low fluorescence in the negative RLE-6TN cells. Therefore, the strong fluorescence from GO and ZnO was likely due to both the matrix effects and the miR-21 dependent reaction, and only the PDANs probe displayed high specificity, which is crucial for tumor diagnostics.

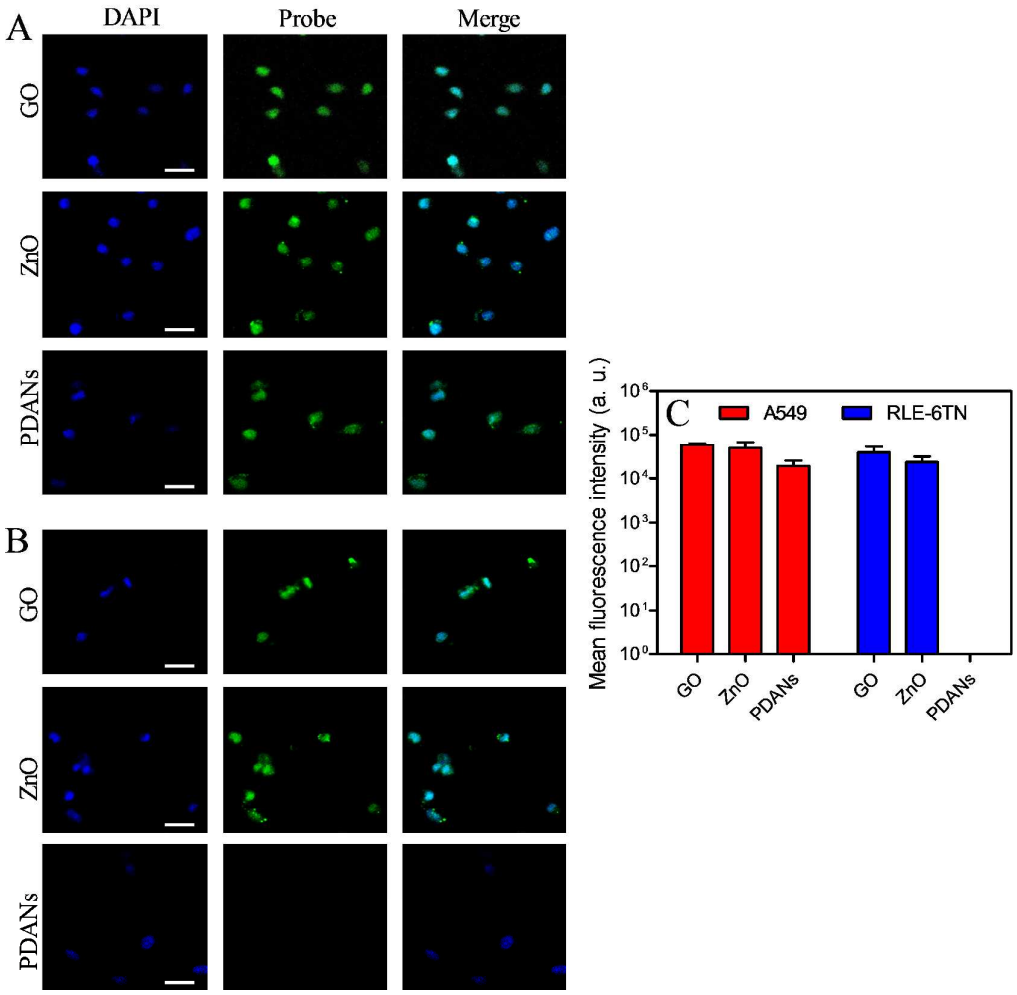

Figure 5. Confocal fluorescence micrographs of the three nanoprobes for miR-21 detection in (A) A549 cancer cells, and (B) RLE-6TN normal cells. (C) The quantified fluorescence intensities of each nanoprobe in both A549 and RLE-6TN cells. The scale bar is 50 μm.

Ca^{2+} coordination mediated adsorption. After demonstrating highly robust DNA detection, we wanted to understand the mechanism for DNA adsorption by PDANs that may explain its excellent analytical performance. Our adsorption studies in Figure 2 have pointed to the importance of polyvalent cations.

To confirm the role of Ca^{2+} on DNA adsorption, XPS experiment was carried out to explore the surface elemental composition (Figure 6A). The PDANs showed three typical peaks representing carbon, oxygen and nitrogen, respectively. After mixing

with DNA, no noticeable change was observed, indicating no DNA adsorption. After incubating with Ca^{2+}, a new peak of Ca 2p emerged, implying Ca^{2+} doping on PDAN surface. Note that PDANs@Ca^{2+} sample has been washed several times prior to XPS characterization to remove loosely bound Ca^{2+}. From the magnified peak region at ca. 346-352 eV, the Ca^{2+} peak was clearly present. Based on the peak intensity, the surface molar ratio of oxygen-to-calcium was calculated to be 9:1. While at this ratio the PDANs were still negatively charged (Figure S9), and the surface oxygen was far from saturated by Ca^{2+}, rapid DNA adsorption was achieved (Figure 2D). Therefore, the role of Ca^{2+} was not for charge reversal, and electrostatic interaction cannot explain DNA adsorption. Finally, we incubated the PDANs with DNA in presence of Ca^{2+}, and the resulting nanoparticles showed two new peaks assigned to Ca 2p and P 2p, respectively. The P 2p peak was from the DNA phosphate backbone, which clearly demonstrated successful adsorption of DNA on PDANs and the role of Ca^{2+} for DNA binding.

After understanding the surface of PDANs for DNA adsorption, we then investigated the adsorption force. Typically, the nucleobases and phosphate backbone are the two main components responsible for DNA adsorption. To find out which one is more important in this case, desorption studies were performed by adding different competing agents. We first studied DNA desorption from PDANs in the presence of inorganic phosphate, and the fluorescence remained at background level with up to 10 mM phosphate (Figure 6B), indicating DNA adsorption was not forced by the phosphate backbone.

We then probed the nucleobase binding by using the free nucleoside. Since FAM-A_{15} DNA was adsorbed on Ca^{2+} doped PDANs, adenosine was added as a competing ligand. Interestingly, we observed [adenosine]-dependent fluorescence increase, implying DNA desorption from PDANs (Figure 6C). Therefore, the adenine base played an important role for DNA adsorption. We also tested other nucleosides, and adenosine was the most efficient (Figure S10). Thymine induced a moderate DNA desorption, while almost no DNA desorption was observed with cytidine.

Previous studies have indicated that PDANs would interact with guest molecules

through hydrogen bonding.[60, 61] To explore whether hydrogen bonding has any effect on DNA binding, urea was added as a strong hydrogen bonding disruptor.[22] Almost no DNA detached from the PDANs with up to 0.5 M urea (Figure S11), suggesting the weak contribution of hydrogen bonding.

To further confirm the critical role of Ca^{2+} on DNA binding, we finally used EDTA as competing ligand, a strong chelator for multivalent metal ions. EDTA could displace DNA from the PDANs in a concentration-dependent manner, and over 60% of the DNA was desorbed in the presence of 4 mM EDTA (Figure S12). The EDTA induced DNA desorption was attributed to its extraction of Ca^{2+} from the PDANs, which confirmed Ca^{2+}-mediated DNA adsorption.

Taken together, Ca^{2+} was likely to mediate DNA adsorption on PDANs *via* the DNA base. As a hard Lewis acid, Ca^{2+} can strongly bind to phosphate (a hard Lewis base) according to the Hard-Soft-Acid-Base theory. For example, calcium phosphate nanoparticles preferentially interact with the phosphate backbone of DNA through surface Ca^{2+}, resulting in DNA adsorption.[62] However, our data showed that DNA phosphate backbone was not much responsible for DNA adsorption by Ca^{2+} doped PDANs. It is likely that the binding between Ca^{2+} and DNA phosphate was cancelled out by the electrostatic repulsion between the phosphate and the particle surface. Using base coordination to bind had a lower charge repulsion.

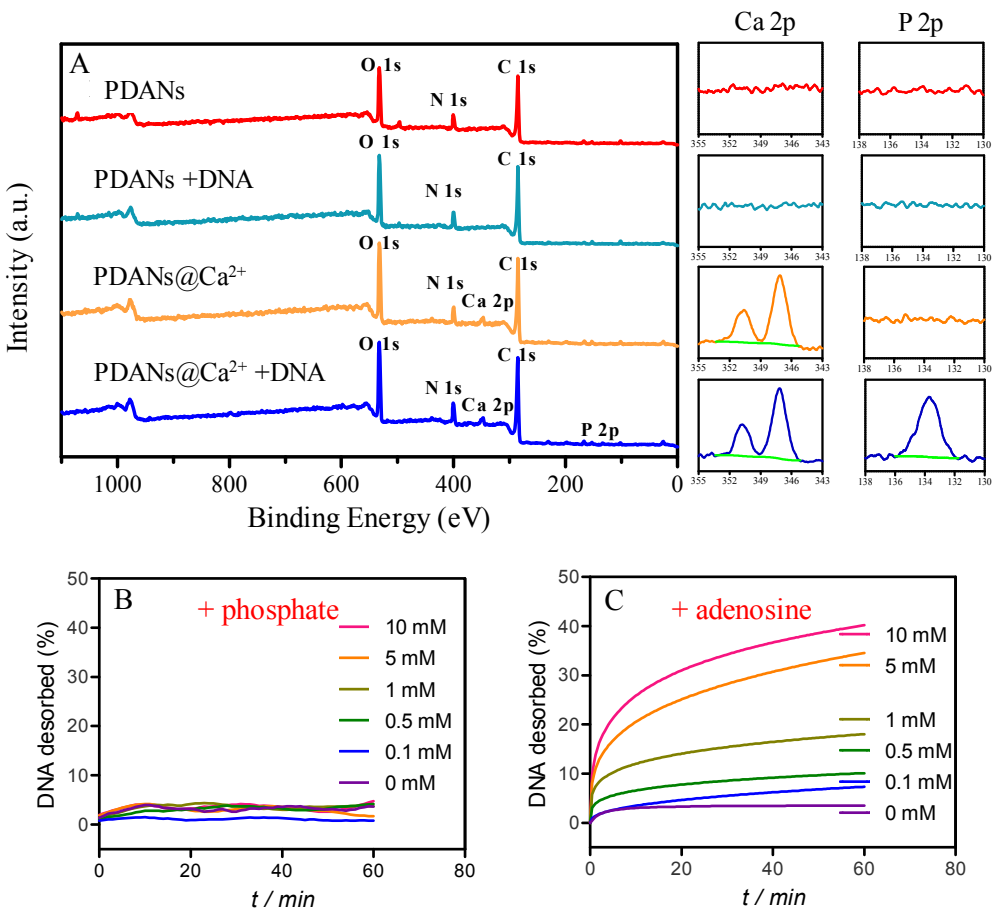

Figure 6. (A) XPS spectra of the PDANs or the PDAN/DNA mixture in absence or presence of Ca^{2+}. The desorption kinetics of DNA from PDANs in the presence of various concentrations of (B) inorganic phosphate, and (C) adenosine.

Other polyvalent metals. In addition to Ca^{2+}, we also tested DNA adsorption in the presence of a few other polyvalent metal ions. In this case Cu^{2+} and Ce^{3+} were chosen. Cu^{2+} is a soft Lewis acid while Ce^{3+} is strong a hard Lewis acid (much stronger than Ca^{2+}).[63] Since these two metals strongly quench FAM, we chose to use a Cy3-labeled DNA for them. Cu^{2+} and Ce^{3+} also induced DNA adsorption on PDANs with even better efficiencies than that of Ca^{2+} (Figure S13). This can be ascribed to their higher binding affinity with DNA and/or the PDANs.[7] The stronger DNA binding can be further evidenced by the fact that even 50 nM cDNA failed to dissociate the probe DNA from Cu^{2+}/Ce^{3+} doped PDANs (Figure S14). Therefore, PDANs@Ca^{2+}/DNA is a better choice for sensing applications. These results further

demonstrated that polyvalent metal ions are required for sufficient DNA adsorption on PDANs. Compared with monovalent salts that act merely as diffusive charges, divalent metals can coordinate with both PDANs and DNA for stronger interactions.

Interestingly, the DNA/PDAN conjugates prepared by these two metals displayed quite different desorption trends upon addition of both phosphate and adenosine (Figure 7A and 7B). For Cu^{2+}-mediated conjugation, DNA was desorbed by adenosine but not by phosphate, similar to the case of Ca^{2+}. For the Ce^{3+} sample, in contrast, DNA was almost fully desorbed in 5 min after introducing phosphate but remained stable with adenosine, which strongly suggests the phosphate backbone binding. The interaction of DNA phosphate backbone with Ce^{3+} is much stronger than that with Ca^{2+}.[63] Therefore, DNA binding on the PDANs can be controlled by simply varying the doping metal ions.

The type of cation is critical for DNA adsorption on PDANs, suggesting that cations are an integrated part of the attractive force for DNA adsorption. This is quite different from most other nanomaterials. For example, AuNPs adsorb DNA *via* DNA base coordination, which is a very strong force. Therefore, as long as the DNA can approach the surface, adsorption can take place.[46, 50, 64, 65] Similarly, for metal (oxide) nanoparticles, the particle surface is abundant of metal elements for DNA coordination/binding, while GO can interact with DNA through π-π stacking and hydrogen bonding.[23] In these materials, metal ions mainly screen charge repulsion. For PDANs, on the other hand, polyvalent metals are required to produce an attractive adsorption force to bridge DNA and PDAN. While PDANs were also reported to interact with guest molecules through π-π stacking and hydrogen bonding,[61] they did not appear to be as important as metal coordination in our system.

Based on all above observations, we proposed the mechanism of DNA adsorption on PDANs (Figure 7C). Polyvalent metal ions mediate the adsorption of DNA on PDANs, and the surface catechol groups on PDANs provide sites for metal coordination, which enables highly stable DNA binding against various biological molecules, such as BSA, FBS and inorganic phosphate (Figure 3). Such DNA binding mechanism is quite distinct from other nanomaterials. As adsorption is realized by

metal coordination, metal ions can be used to modulate binding. For example, the DNA binding sites and affinities are very different for Ce^{3+} and Ca^{2+} doped PDANs.

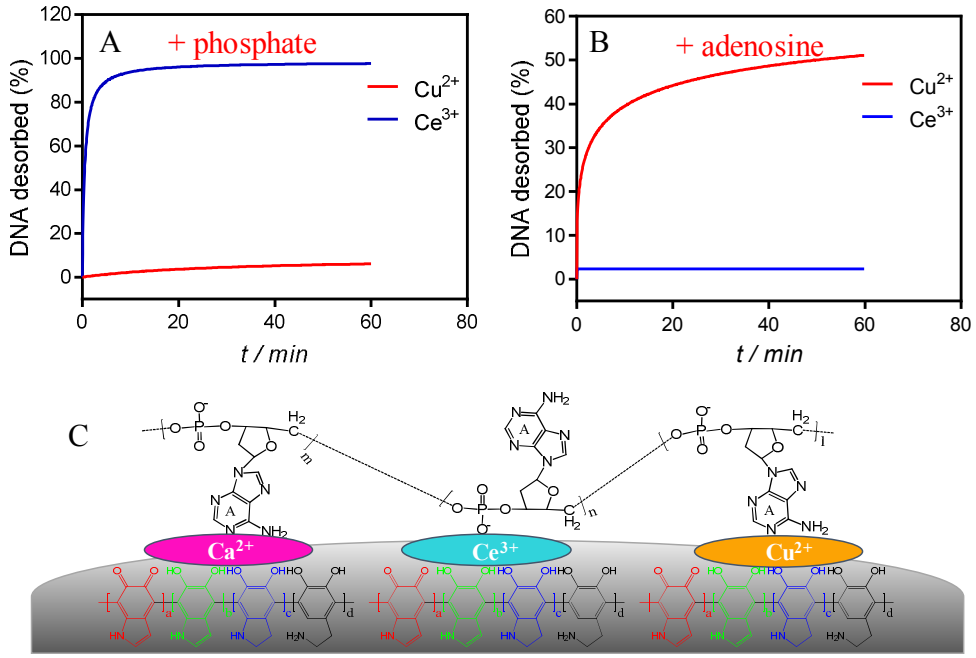

Figure 7. The kinetics of DNA desorption from PDANs (adsorbed by 50 μM Cu^{2+} or Ce^{3+}) in presence of (A) 10 mM inorganic phosphate, and (B) 10 mM adenosine. (C) The proposed mechanism of DNA adsorption on PDANs doped with various metal ions. For the case of Ca^{2+} and Cu^{2+}, DNA is adsorbed through nucleobase coordination, while for Ce^{3+}, DNA adsorption is achieved through phosphate backbone binding.

Conclusions.

In summary, we demonstrated robust DNA/PDAN-based sensors in biological samples, which was attributable to the adsorption mechanism of DNA on PDANs. Compared to other nanomaterials that directly adsorb DNA, PDANs bind DNA *via* metal coordination. Such a distinct mechanism endows DNA/PDAN with several interesting properties. First, the binding site and affinity of DNA on PDANs can be controlled by using different metals, which is difficult to realize by other nanomaterials. More importantly, with metal coordination mediated conjugation, the DNA/PDAN system can resist displacement by various competing biological ligands,

which is crucial for its biological applications. Using DNA/PDANs as probes, detection of target DNA in serum and imaging of tumor-related microRNA in living cells were demonstrated, while ZnO and GO based sensors adsorbed with the same probe DNA were more susceptible to false signals. This study will facilitate the design of more sophisticated and practically useful DNA-based biosensors in complex biological samples, and smart nano-assembles directed by DNA.

Materials and methods.

Chemicals. All of the DNA samples were purchased from Sangon Biotech Co., Ltd. (Shanghai, China) and purified by high-performance liquid chromatography (HPLC). Dopamine hydrochloride was purchased from Energy Chemical (Shanghai, China), and 4-(2-hydroxyethyl)-piperazine-1-ethanesulfonic acid (HEPES) was from BioFroxx (Einhausen, Germany). Sodium acetate, sodium citrate, Tris(hydroxymethyl)aminomethane (Tris), sodium dihydrogen phosphate dihydrate and urea were from Sinopharm Chemical Reagent Co. Ltd (Shanghai, China). Nucleosides and Ethylenediaminetetraacetic acid dipotassium salt dihydrate (EDTA-2K) were from Sigma-Aldrich and metal chloride salts were from Macklin (purity > 99.9 %) (Shanghai, China). RPMI 1640 Medium, fetal bovine serum (FBS) and 0.25% (w/v) trypsin solution were purchased from Gibco (Grand Island, NY, USA). Serum was fresh prepared by centrifugation (1000 rpm) of blood collected from orbital vein of sprague-dawley rats (The experiment was approved by Ethics Committee for research in animal subjects at Xiangya School of Pharmaceutical Sciences of Central South University). Penicillin-streptomycin solution and 4′, 6-diamidino-2-phenylindole (DAPI) were provided by Solarbio Biotech, Co., Ltd. (Beijing, China). Glass bottom cell culture dishes (Φ20 mm) were purchased from Nest Biotechnology Co., Ltd. (Wuxi, China). Milli-Q water (electric resistance >18.25 MΩ) was used for all of the experiments.

Table 1. The DNA sequences and modifications used in this work. The underlined bases highlight the position of mismatch.

DNA name	sequence and modifications (5′-3′)
FAM-A_{15}	FAM-AAAAAAAAAAAAAAA
FAM-T_{15}	FAM-TTTTTTTTTTTTTTT
FAM-C_{15}	FAM-CCCCCCCCCCCCCCC
FAM-G_{15}	FAM-GGGGGGGGGGGGGGG
FAM-A_8	FAM-AAAAAAAA
FAM-A_{30}	FAM-AAAAAAAAAAAAAAAAAAAAAAAAAAAAAA
Cy3-A_{15}	Cy3-AAAAAAAAAAAAAAA
Alexa Fluor 488-A_{15}	Alexa Fluor 488-AAAAAAAAAAAAAAA
A_{15}	AAAAAAAAAAAAAAA
T_{15}	TTTTTTTTTTTTTTT
C_{15}	CCCCCCCCCCCCCCC
FAM-probe DNA	FAM-ACGCATCTGTGAAGAGAACCTGGG
cDNA	CCCAGGTTCTCTTCACAGATGCGT
misDNA1	CCCAGGTTCTCTTCACACATGCGT
FAM-miR21 DNA	TCAACATCAGTCTGATAAGCTA

Cell lines and culture conditions. The Human non-small-cell carcinoma (A549) cells and rat lung epithelial-T-antigen negative (RLE-6TN) normal cells were obtained from Xiangya Central Experiment Laboratory (Hunan, China), and grown in complete RPMI-1640 medium (with 10% (v/v) FBS, 1% Penicillin-streptomycin solution (100 U/mL)) at 37 ºC in a humidified atmosphere with 5% CO_2.

Synthesis and characterization of PDANs. Under vigorous stirring, 80 mg dopamine hydrochloride was added to the alcohol co-solvent (20 mL alcohol, 100 mL 10 mM Tris base), followed by 72 h reaction in the dark at room temperature. The PDANs were collected by centrifugation at 20000 rpm for 30 min and washed with Milli-Q water for three times, and then re-dispersed in Milli-Q water for the subsequent experiments. The ζ-potential and dynamic size of the as-prepared PDANs were measured by Zetasizer Nano 90 (Malvern), and the morphology were

characterized using transmission electron microscopy (TEM) (Philips CM10).

DNA adsorption on PDANs. For a typical experiment, 10 nM FAM-labeled DNA (FAM-A_{15}) was quickly added to 50 μg/mL PDANs with different metal concentrations (pH 7.6, buffered by 10 mM HEPES), and the fluorescence intensity (Ex = 470 nm, Em = 518 nm) was monitored for 30 min to track the adsorption kinetics.

DNA displacement studies. Typically, 10 μL of various desorption reagents were quickly added to 90 μL the prepared DNA/PDANs conjugate (10 mM HEPES buffer, pH 7.6, 2 mM Ca^{2+}, DNA = 10 nM), and the reaction kinetics were monitored using a fluorescence microplate reader (Ex = 470 nm, Em = 518 nm). The desorption reagents included phosphate (0, 0.1, 0.5, 1, 5 and 10 mM), adenosine (0, 0.1, 0.5, 1, 5 and 10 mM), thymine (10 mM) and cytidine (10 mM), 15-nt DNA homopolymers (100 nM), Urea (0, 10 nM, 1 μM, 1, 100 and 500 mM), 100 μg/mL BSA and 0.5% FBS and EDTA (1-4 mM). For comparison, the DNA displacement experiments were also performed for DNA/ZnO conjugate and DNA/GO conjugate in presence of 100 μg/mL BSA, 0.5% FBS and 10 mM phosphate. The DNA/ZnO conjugate was prepared by mixing 10 nM FAM-A_{15} with 15 μg/mL ZnO (10 mM HEPES, pH 7.6, 150 mM NaCl), while DNA/GO conjugate was prepared by adding 10 nM FAM-A_{15} to 2 μg/mL GO (10 mM HEPES, pH 7.6, 300 mM NaCl), and each were incubated for 120 min for sufficient DNA adsorption.

DNA detection. The nanoprobe was prepared by mixing 1 μM FAM-probe DNA with PDANs (100 μg/mL) in buffer A (10 mM HEPES, pH 7.6, 2 mM Ca^{2+}) for 24 h, followed by centrifugation (20000 rpm) for 30 min to remove free FAM-probe DNA, and the conjugate was re-dispersed in buffer A. Various concentrations of cDNA were added, and the fluorescence was measured after incubating for 30 min. To test the specificity, 50 nM cDNA, misDNA, A_{15}, T_{15} or C_{15} was used.

To detect cDNA in BSA or serum, the nanoprobe was prepared by the same method, and re-dispersed in buffer A supplied with 100 μg/mL BSA or 0.5% serum. The detection of cDNA in phosphate was performed in 10 mM phosphate buffer (pH 7.6, 5 mM Mg^{2+}).

Imaging of microRNA in living cells. The nanoprobes were prepared by adsorbing 100 nM FAM-miR21 DNA and were diluted with fresh culture medium. The cells were seeded in cell culture dishes and grown for 24 h until approximately 90% confluent. After removing the medium and washing with PBS, the culture medium was replaced by nanoprobes for 8 h incubation. Then, the cells were washed with 1 × PBS for three times and stained with DAPI for confocal scanning laser microscope investigation.

XPS characterization. PDANs@Ca^{2+}/DNA complex was prepared by mixing PDANs (1 mg/mL) with Ca^{2+} (20 mM) and DNA (A_{15}, 5 μM) in 10 mM HEPES (pH 7.6). After incubation, the PDANs@Ca^{2+}/DNA were collected by centrifugation (20000 rpm) to remove free Ca^{2+} and DNA, and then freeze-dried for XPS (Axis-Ultra DLD) measurement. PDANs, PDANs@Ca^{2+} and PDANs/DNA samples were subjected to the same steps without adding Ca^{2+} and/or DNA.

ASSOCIATED CONTENT

Supporting Information Available

Information and analysis related to UV-Vis, FT-IR and Raman characterizations PDANs; DLS size and ζ-potential of PDANs; the FAM fluorescence quenching efficiency by different metal ions; DNA adsorption kinetics as a function of pH; DNA desorption by 0.5% FBS, nucleosides, urea and EDTA; RT-PCR for the quantification of relative miR-21 level in A549 and RLE-6TN cells; MTT assay and cell morphologies after treatment with different nanoprobes; ζ-potential of PDANs after incubating with different Ca^{2+} concentrations; DNA adsorption induced by 50 μM Cu^{2+} or Ce^{3+}; Performances of Cu^{2+}/Ce^{3+} doped PDANs probes for target DNA detection. This material is available free of charge *via* the Internet at http://pubs.acs.org.

Conflict of interest

The authors declare no conflict of interest.

AUTHOR INFORMATION

Corresponding Author

*E-mail: zhouwenhuyaoji@163.com

ORCID

Wenhu Zhou: 0000-0003-3794-661X

Juewen Liu: 0000-0001-5918-9336

Acknowledgments

This work was supported by Innovation-Driven Project of Central South University (No. 20170030010004), National Natural Science Foundation of China (No. 81573374), Key Laboratory Breeding Base of Hunan Oriented Fundamental and Applied Research in Innovative Pharmaceutics (No. 2016TP1029), and Hunan Engineering Research Center for Optimization of Drug Formulation and Early Clinical Evaluation (No. 2015TP2005).

References.

1. Lang, K.; Chin, J. W. Bioorthogonal Reactions for Labeling Proteins. *ACS Chem. Biol.* 2014, 9, 16-20.

2. Gupta, A.; Das, R.; Tonga, G. Y.; Mizuhara, T.; Rotello, V. M. Charge-Switchable Nanozymes for Bioorthogonal Imaging of Biofilm-Associated Infections. *ACS Nano* 2018, 12, 89-94.

3. Jones, M. R.; Seeman, N. C.; Mirkin, C. A. Programmable Materials and the Nature of the DNA Bond. *Science* 2015, 347, 1260901-1260911.

4. Nykypanchuk, D.; Maye, M. M.; van der Lelie, D.; Gang, O. DNA-Guided Crystallization of Colloidal Nanoparticles. *Nature* 2008, 451, 549-522.

5. Lan, X.; Wang, Q. DNA-Programmed Self-Assembly of Photonic Nanoarchitectures. *Npg Asia Materials* 2014, 6, e97.

6. Lu, Y.; Liu, J. Smart Nanomaterials Inspired by Biology: Dynamic Assembly of Error-Free Nanomaterials in Response to Multiple Chemical and Biological Stimuli. *Acc. Chem. Res.* 2007, 40, 315-323.

7. Zhou, W.; Saran, R.; Liu, J. Metal Sensing by DNA. *Chem. Rev.* 2017, 117, 8272-8325.

8. Song, S.; Qin, Y.; He, Y.; Huang, Q.; Fan, C.; Chen, H.-Y. Functional Nanoprobes for Ultrasensitive Detection of Biomolecules. *Chem. Soc. Rev.* 2010, 39, 4234-4243.

9. Wang, H.; Yang, R.; Yang, L.; Tan, W. Nucleic Acid Conjugated Nanomaterials for Enhanced Molecular Recognition. *ACS Nano* 2009, 3, 2451-2460.

10. Liu, J.; Cao, Z.; Lu, Y. Functional Nucleic Acid Sensors. *Chem. Rev.* 2009, 109, 1948–1998.

11. Rosi, N. L.; Mirkin, C. A. Nanostructures in Biodiagnostics. *Chem. Rev.* 2005, 105, 1547-1562.

12. Giljohann, D. A.; Seferos, D. S.; Daniel, W. L.; Massich, M. D.; Patel, P. C.; Mirkin, C. A. Gold Nanoparticles for Biology and Medicine. *Angew. Chem. Int. Ed.* 2010, 49, 3280-3294.

13. Fan, H. H.; Zhang, X. B.; Lu, Y. Recent Advances in DNAzyme-Based Gene Silencing. *Sci. China-Chem.* 2017, 60, 591-601.

14. Mirkin, C. A.; Letsinger, R. L.; Mucic, R. C.; Storhoff, J. J. A DNA-Based Method for Rationally Assembling Nanoparticles into Macroscopic Materials. *Nature* 1996, 382, 607-609.

15. Liu, B.; Liu, J. Comprehensive Screen of Metal Oxide Nanoparticles for DNA Adsorption, Fluorescence Quenching, and Anion Discrimination. *ACS Appl. Mater. Interfaces* 2015, 7, 24833-24838.

16. Liu, B.; Sun, Z.; Huang, P.-J. J.; Liu, J. Hydrogen Peroxide Displacing DNA from Nanoceria: Mechanism and Detection of Glucose in Serum. *J. Am. Chem. Soc.* 2015, 137, 1290-1295.

17. Zhou, Y. B.; Huang, Z. C.; Yang, R. H.; Liu, J. W. Selection and Screening of DNA Aptamers for Inorganic Nanomaterials. *Chem. Eur. J.* 2018, 24, 2525-2532.

18. Mitchell, G. P.; Mirkin, C. A.; Letsinger, R. L. Programmed Assembly of DNA Functionalized Quantum Dots. *J. Am. Chem. Soc.* 1999, 121, 8122-8123.

19. Lu, C. H.; Yang, H. H.; Zhu, C. L.; Chen, X.; Chen, G. N. A Graphene Platform for Sensing Biomolecules. *Angew. Chem. Int. Ed.* 2009, 48, 4785-4787.

20. Sun, H. J.; Ren, J. S.; Qu, X. G. Carbon Nanomaterials and DNA: from Molecular Recognition to Applications. *Acc. Chem. Res.* 2016, 49, 461-470.

21. Wu, M.; Kempaiah, R.; Huang, P.-J. J.; Maheshwari, V.; Liu, J. Adsorption and Desorption of DNA on Graphene Oxide Studied by Fluorescently Labeled Oligonucleotides. *Langmuir* 2011, 27, 2731-2738.

22. Park, J. S.; Na, H.-K.; Min, D.-H.; Kim, D.-E. Desorption of Single-Stranded Nucleic Acids from Graphene Oxide by Disruption of Hydrogen Bonding. *Analyst* 2013, 138, 1745-1749.

23. Varghese, N.; Mogera, U.; Govindaraj, A.; Das, A.; Maiti, P. K.; Sood, A. K.; Rao, C. N. R. Binding of DNA Nucleobases and Nucleosides with Graphene. *Chemphyschem* 2009, 10, 206-210.

24. De Leo, F.; Magistrato, A.; Bonifazi, D. Interfacing Proteins with Graphitic Nanomaterials: from Spontaneous Attraction to Tailored Assemblies. *Chem. Soc. Rev.* 2015, 44, 6916-6953.

25. Liu, J.; Fu, S.; Yuan, B.; Li, Y.; Deng, Z. Toward a Universal "Adhesive Nanosheet" for the Assembly of Multiple Nanoparticles Based on a Protein-Induced Reduction/Decoration of Graphene Oxide. *J. Am. Chem. Soc.* 2010, 132, 7279-7281.

26. Liu, B.; Ma, L.; Huang, Z.; Hu, H.; Wu, P.; Liu, J. Janus DNA Orthogonal Adsorption of Graphene Oxide and Metal Oxide Nanoparticles Enabling Stable Sensing in Serum. *Mater. Horiz.* 2018, 5, 65-69.

27. Tan, X.; Chen, T.; Xiong, X.; Mao, Y.; Zhu, G.; Yasun, E.; Li, C.; Zhu, Z.; Tan, W. Semiquantification of ATP in Live Cells Using Nonspecific Desorption of DNA from Graphene Oxide as the Internal Reference. *Anal. Chem.* 2012, 84, 8622-8627.

28. Huang, P.-J. J.; Liu, J. Molecular Beacon Lighting up on Graphene Oxide. *Anal. Chem.* 2012, 84, 4192-4198.

29. He, C. B.; Liu, D. M.; Lin, W. B. Nanomedicine Applications of Hybrid Nanomaterials Built from Metal-Ligand Coordination Bonds: Nanoscale Metal-Organic Frameworks and Nanoscale Coordination Polymers. *Chem. Rev.* 2015, 115, 11079-11108.

30. Liu, M.; Zeng, G.; Wang, K.; Wan, Q.; Tao, L.; Zhang, X.; Wei, Y. Recent Developments in Polydopamine: An Emerging Soft Matter for Surface Modification and Biomedical Applications. *Nanoscale* 2016, 8, 16819-16840.

31. Lynge, M. E.; van der Westen, R.; Postma, A.; Stadler, B. Polydopamine-A Nature-Inspired Polymer Coating for Biomedical Science. *Nanoscale* 2011, 3, 4916-4928.

32. Liu, Y.; Ai, K.; Lu, L. Polydopamine and Its Derivative Materials: Synthesis and Promising

Applications in Energy, Environmental, and Biomedical Fields. *Chem. Rev.* 2014, 114, 5057-5115.

33. Zhong, X.; Yang, K.; Dong, Z.; Yi, X.; Wang, Y.; Ge, C.; Zhao, Y.; Liu, Z. Polydopamine as A Biocompatible Multifunctional Nanocarrier for Combined Radioisotope Therapy and Chemotherapy of Cancer. *Adv. Funct. Mater.* 2015, 25, 7327-7336.

34. Qiang, W.; Li, W.; Li, X.; Chen, X.; Xu, D. Bioinspired Polydopamine Nanospheres: A Superquencher for Fluorescence Sensing of Biomolecules. *Chem. Sci.* 2014, 5, 3018-3024.

35. Qiang, W. B.; Hu, H. T.; Sun, L.; Li, H.; Xu, D. K. Aptamer/Polydopamine Nanospheres Nanocomplex for *in Situ* Molecular Sensing in Living Cells. *Anal. Chem.* 2015, 87, 12190-12196.

36. He, D.; He, X.; Yang, X.; Li, H.-W. A Smart ZnO@Polydopamine-Nucleic Acid Nanosystem for Ultrasensitive Live Cell mRNA Imaging by the Target-Triggered Intracellular Self-Assembly of Active DNAzyme Nanostructures. *Chem. Sci.* 2017, 8, 2832-2840.

37. Choi, C. K. K.; Li, J. M.; Wei, K. C.; Xu, Y. J.; Ho, L. W. C.; Zhu, M. L.; To, K. K. W.; Choi, C. H. J.; Bian, L. M. A Gold@Polydopamine Core-Shell Nanoprobe for Long-Term Intracellular Detection of MicroRNAs in Differentiating Stem Cells. *J. Am. Chem. Soc.* 2015, 137, 7337-7346.

38. Lin, L. S.; Cong, Z. X.; Cao, J. B.; Ke, K. M.; Peng, Q. L.; Gao, J. H.; Yang, H. H.; Liu, G.; Chen, X. Y. Multifunctional Fe3O4@Polydopamine Core-Shell Nanocomposites for Intracellular mRNA Detection and Imaging-Guided Photothermal Therapy. *ACS Nano* 2014, 8, 3876-3883.

39. Zeng, H. B.; Hwang, D. S.; Israelachvili, J. N.; Waite, J. H. Strong Reversible Fe^{3+}-Mediated Bridging between Dopa-Containing Protein Films in Water. *Proc. Natl. Acad. Sci. U. S. A.* 2010, 107, 12850-12853.

40. Holten-Andersen, N.; Harrington, M. J.; Birkedal, H.; Lee, B. P.; Messersmith, P. B.; Lee, K. Y. C.; Waite, J. H. pH-Induced Metal-Ligand Cross-Links Inspired by Mussel Yield Self-Healing Polymer Networks with Near-Covalent Elastic Moduli. *Proc. Natl. Acad. Sci. U. S. A.* 2011, 108, 2651-2655.

41. Ge, R.; Lin, M.; Li, X.; Liu, S. W.; Wang, W. J.; Li, S. Y.; Zhang, X.; Liu, Y.; Liu, L. D.; Shi, F.; Sun, H. C.; Zhang, H.; Yang, B. Cu^{2+}-Loaded Polydopamine Nanoparticles for Magnetic Resonance Imaging-Guided pH- and Near-Infrared-Light-Stimulated Thermochemotherapy. *ACS Appl. Mater. Interfaces* 2017, 9, 19706-19716.

42. Zheng, X. Y.; Zhang, J. X.; Wang, J.; Qi, X. Q.; Rosenholm, J. M.; Cai, K. Y. Polydopamine Coatings in Confined Nanopore Space: Toward Improved Retention and Release of Hydrophilic Cargo. *J. Phys. Chem. C* 2015, 119, 24512-24521.

43. Yan, J.; Yang, L. P.; Lin, M. F.; Ma, J.; Lu, X. H.; Lee, P. S. Polydopamine Spheres as Active Templates for Convenient Synthesis of Various Nanostructures. *Small* 2013, 9, 596-603.

44. Liu, Y. L.; Ai, K. L.; Liu, J. H.; Deng, M.; He, Y. Y.; Lu, L. H. Dopamine-Melanin Colloidal Nanospheres: An Efficient Near-Infrared Photothermal Therapeutic Agent for *in Vivo* Cancer Therapy. *Adv. Mater.* 2013, 25, 1353-1359.

45. Elghanian, R.; Storhoff, J. J.; Mucic, R. C.; Letsinger, R. L.; Mirkin, C. A. Selective Colorimetric Detection of Polynucleotides Based on the Distance-Dependent Optical Properties of Gold Nanoparticles. *Science* 1997, 277, 1078-1081.

46. Storhoff, J. J.; Elghanian, R.; Mucic, R. C.; Mirkin, C. A.; Letsinger, R. L. One-Pot Colorimetric Differentiation of Polynucleotides with Single Base Imperfections Using Gold Nanoparticle Probes. *J. Am. Chem. Soc.* 1998, 120, 1959-1964.

47. Karabulut, E.; Pettersson, T.; Ankerfors, M.; Wagberg, L. Adhesive Layer-by-Layer Films of Carboxymethylated Cellulose Nanofibril Dopamine Covalent Bioconjugates Inspired by Marine Mussel Threads. *ACS Nano* 2012, 6, 4731-4739.

48. Han, Y. Y.; Wu, X. D.; Zhang, X. X.; Zhou, Z. H.; Lu, C. H. Dual Functional Biocomposites Based on Polydopamine Modified Cellulose Nanocrystal for Fe^{3+}-Pollutant Detecting and Autoblocking. *ACS Sustain. Chem. Eng.* 2016, 4, 5667-5673.

49. Zhao, Z.; Chen, H. D.; Zhang, H.; Ma, L. N.; Wang, Z. X. Polyacrylamide-Phytic Acid-Polydopamine Conducting Porous Hydrogel for Rapid Detection and Removal of Copper (II) Ions. *Biosens. Bioelectron.* 2017, 91, 306-312.

50. Zhang, X.; Servos, M. R.; Liu, J. Instantaneous and Quantitative Functionalization of Gold Nanoparticles with Thiolated DNA Using a pH-Assisted and Surfactant-Free Route. *J. Am. Chem. Soc.* 2012, 134, 7266–7269.

51. Kim, S. N.; Kuang, Z.; Slocik, J. M.; Jones, S. E.; Cui, Y.; Farmer, B. L.; McAlpine, M. C.; Naik, R. R. Preferential Binding of Peptides to Graphene Edges and Planes. *J. Am. Chem. Soc.* 2011, 133, 14480-14483.

52. Katoch, J.; Kim, S. N.; Kuang, Z.; Farmer, B. L.; Naik, R. R.; Tatulian, S. A.; Ishigami, M. Structure of A Peptide Adsorbed on Graphene and Graphite. *Nano Lett.* 2012, 12, 2342-2346.

53. Zhou, J.; Xu, X.; Liu, W.; Liu, X.; Nie, Z.; Qing, M.; Nie, L.; Yao, S. Graphene Oxide–Peptide Nanocomplex as A Versatile Fluorescence Probe of Protein Kinase Activity Based on Phosphorylation Protection against Carboxypeptidase Digestion. *Anal. Chem.* 2013, 85, 5746-5754.

54. Zhou, W.; Chen, Q.; Huang, P.-J. J.; Ding, J.; Liu, J. DNAzyme Hybridization, Cleavage, Degradation, and Sensing in Undiluted Human Blood Serum. *Anal. Chem.* 2015, 87, 4001-4007.

55. Bartel, D. P. MicroRNAs: Genomics, Biogenesis, Mechanism, and Function. *Cell* 2004, 116, 281-297.

56. Pfeffer, S. R.; Yang, C. H.; Pfeffer, L. M. The Role of miR-21 in Cancer. *Drug Dev. Res.* 2015, 76, 270-277.

57. Li, S.; Liu, C.; Gong, H.; Chen, C.; Chen, X.; Cai, C. Simple G-Quadruplex-Based 2-Aminopurine Fluorescence Probe for Highly Sensitive and Amplified Detection of MicroRNA-21. *Talanta* 2018, 178, 974-979.

58. Oudeng, G.; Au, M. T.; Shi, J. Y.; Wen, C. Y.; Yang, M. One-Step *in Situ* Detection of miRNA-21 Expression in Single Cancer Cells Based on Biofunctionalized MoS_2 Nanosheets. *ACS Appl. Mater. Interfaces* 2018, 10, 350-360.

59. Kangkamano, T.; Numnuam, A.; Limbut, W.; Kanatharana, P.; Vilaivan, T.; Thavarungkul, P. Pyrrolidinyl PNA Polypyrrole/Silver Nanofoam Electrode as A Novel Label-Free Electrochemical miRNA-21 Biosensor. *Biosens. Bioelectron.* 2018, 102, 217-225.

60. Wang, X. Y.; Zhang, J. S.; Wang, Y. T.; Wang, C. P.; Xiao, J. R.; Zhang, Q.; Cheng, Y. Y. Multi-Responsive Photothermal-Chemotherapy with Drug-Loaded Melanin-Like Nanoparticles for Synergetic Tumor Ablation. *Biomaterials* 2016, 81, 114-124.

61. Li, W.; Wang, Z.; Hao, S.-J.; He, H.; Wan, Y.; Zhu, C.; Sun, L.; Cheng, G.; Zheng, S.-Y. Mitochondria-Targeting Polydopamine Nanoparticles to Deliver Doxorubicin for Overcoming Drug Resistance. *ACS Appl. Mater. Interfaces* 2017, 9, 16794-16803.

62. Wang, L.; Zhang, Z.; Liu, B.; Liu, Y.; Lopez, A.; Wu, J.; Liu, J. Interfacing DNA Oligonucleotides with Calcium Phosphate and Other Metal Phosphates. *Langmuir* 2018, DOI: 10.1021/acs.langmuir.7b03204.

63. Lopez, A.; Liu, J. W. Self-Assembly of Nucleobase, Nucleoside and Nucleotide Coordination Polymers: from Synthesis to Applications. *ChemNanoMat* 2017, 3, 670-684.

64. Liu, B.; Liu, J. Freezing Directed Construction of Bio/Nano Interfaces: Reagentless Conjugation, Denser Spherical Nucleic Acids, and Better Nanoflares. *J. Am. Chem. Soc.* 2017, 139, 9471-9474.

65. Liu, B.; Wu, P.; Huang, Z.; Ma, L.; Liu, J. Bromide as A Robust Backfiller on Gold for Precise Control of DNA Conformation and High Stability of Spherical Nucleic Acids. *J. Am. Chem. Soc.* 2018, 140, 4499-4502.

For Table of Contents Only